pressed at a low level. In the simplest model, CBF1 acts to tether EBNA2 to the promoters of otherwise quiescent target genes. Because EBNA2 contains a transcriptional activation domain (*12*), the promoter-bound protein could act locally to induce transcription in a manner similar to that of conventional transcription factors. By using CBF1 as a target for EBNA2, EBV effectively subverts the ability of B cells to control the expression of these genes. Moreover, EBNA2 might mimic a cellular factor that normally binds CBF1 and activates B cell genes in response to stimuli. This interpretation offers a new focal point for future studies concerning B cell activation.

REFERENCES AND NOTES

1. E. Kieff and D. Liebowitz, in *Virology*, B. N. Fields and D. M. Knipe, Eds. (Raven, New York, 1990), pp. 1889–1920.
2. G. Miller, *ibid.*, pp. 1921–1958.
3. J. I. Cohen, F. Wang, J. Mannick, E. Kieff, *Proc. Natl. Acad. Sci. U.S.A.* **86**, 9558 (1989).
4. W. Hammerschmidt and B. Sugden, *Nature* **340**, 393 (1989).
5. M. Cordier *et al.*, *J. Virol.* **64**, 1002 (1990).
6. R. Fahraeus, A. Jansson, A. Ricksten, A. Sjoblom, L. Rymo, *Proc. Natl. Acad. Sci. U.S.A.* **87**, 7390 (1990).
7. X. W. Jin and S. H. Speck, *J. Virol.* **66**, 2846 (1992).
8. N. S. Sung, S. Kenney, D. Gutsch, J. S. Pagano, *ibid.* **65**, 2164 (1991).
9. F. Wang, H. Kikutani, S. F. Tsang, T. Kishimoto, E. Kieff, *ibid.*, p. 4101.
10. U. Zimber-Strobl *et al.*, *EMBO J.* **12**, 167 (1993).
11. P. D. Ling, D. R. Rawlins, S. D. Hayward, *Proc. Natl. Acad. Sci. U.S.A.* **90**, 9237 (1993).
12. P. D. Ling, J. J. Ryon, S. D. Hayward, *J. Virol.* **67**, 2990 (1993).
13. Abbreviations for the amino acid residues are as follows: C, Cys; D, Asp; E, Glu; F, Phe; G, Gly; H, His; I, Ile; K, Lys; L, Leu; M, Met; P, Pro; Q, Gln; R, Arg; S, Ser; T, Thr; V, Val; W, Trp; and Y, Tyr.
14. N. Matsunami *et al.*, *Nature* **342**, 934 (1989).
15. R. Amakawa *et al.*, *Genomics* **17**, 306 (1993).
16. T. Henkel, P. D. Ling, S. D. Hayward, M. G. Peterson, unpublished data.
17. Y. Hamaguchi, N. Matsunami, Y. Yamamoto, T. Honjo, *Nucleic Acids Res.* **17**, 9015 (1989).
18. Since submission of this manuscript, T. Tun *et al.* [*ibid.* **22**, 965 (1994)] have described CGTGGGAA as the consensus binding site for $RBPJ_{\kappa}$, which is in accordance with our data.
19. F. Schweisguth and J. W. Posakony, *Cell* **69**, 1199 (1992).
20. T. Furukawa, S. Maruyama, M. Kawaichi, T. Honjo, *ibid.*, p. 1191.
21. Y. Hamaguchi *et al.*, *J. Biochem.* **112**, 314 (1992).
22. P. M. Lieberman, J. M. Hardwick, S. D. Hayward, *J. Virol.* **63**, 3040 (1989).
23. E. Schreiber, P. Matthias, M. M. Muller, W. Schaffner, *Nucleic Acids Res.* **17**, 6419 (1989).
24. J. D. Dignam, R. M. Lebovitz, R. G. Roeder, *ibid.* **11**, 1475 (1983).
25. S. P. Jackson and R. Tjian, *Proc. Natl. Acad. Sci. U.S.A.* **86**, 1781 (1989).

26. We are indebted to M. Brasseur for his expertise in peptide separation. We thank S. L. McKnight, K. LaMarco, V. Baichwal, D. Goeddel, and D. Kemp for their critical reading of the manuscript. T.H. was the recipient of a fellowship from the Deutsche Forschungsgemeinschaft. Supported by grants to S.D.H. from NIH (CA42245) and the American Chemical Society (FRA429) and by Tularik Inc.

17 March 1994; accepted 9 May 1994

Magnetoreception in Honeybees

Chin-Yuan Hsu and Chia-Wei Li*

Magnetoreception by honeybees (*Apis mellifera*) is demonstrated by such activities as comb building and homing orientation, which are affected by the geomagnetic field. In other magnetoreceptive species, iron oxide crystals in the form of magnetite have been shown to be necessary for primary detection of magnetic fields. Here it is shown that trophocytes, which are apparently the only iron granule–containing cells in honeybees, contain superparamagnetic magnetite. These cells are innervated by the nervous system, which suggests that trophocytes might be primarily responsible for magnetoreception. Electron microscopy also shows cytoskeletal attachments to the iron granule membrane.

The magnetic field of the Earth influences the behavior and orientation of a variety of organisms, such as magnetotactic bacteria (*1*), algae (*2*), marine mollusks (*3*), honeybees (*4*), hornets (*5*), salmon (*6*), tuna (*7*), turtles (*8*), salamanders (*9*), homing pigeons (*10*), cetaceans (*11*), and human beings (*12*). One of the best understood examples of magnetoreception and magnetonavigation is that of magnetotactic bacteria, whose magnetoreceptors are single-domain particles of magnetite (Fe_3O_4), arranged in a chain along the long axis of each bacterium (*13*). These bacteria swim to the north in the Northern Hemisphere, to the south in the Southern Hemisphere, and in both directions at the geomagnetic equator (*14*). In metazoans, the precise localization of single-domain magnetites and the linkage of these crystals to functioning sensory nerves that transmit magnetic field information to the central nervous system have not been determined, even though single-domain magnetite particles have been extracted from the dermethmoid tissue of the yellowfin tuna (*15*), the forehead of salmon (*16, 17*), the dura mater of green turtles (*8*), and from human brain tissue (*18*).

The existence of a magnetoreceptor in honeybees has been suggested by behavioral and biochemical studies. Worker bees are magnetic (*19*), as measured by superconducing quantum interference devices, and magnetite has been obtained from the abdomens of dried bees, as shown by the abdomen tissue's Curie temperature and magnetization. In honeybees, the only cells that contain iron granules are the trophocytes, which surround each abdominal segment (*20*). Iron deposition in the trophocytes begins on the second day after eclosion, and the iron granule is subsequently formed by the aggregation of dense particles (approximately 7.5 nm in diameter) in the iron deposition vesicles (*21*). However, the iron granules have seemed not to be crystals (*20, 21*) and thus would not be expected to contribute to the measured permanent magnetism. This discrepancy has been accounted for by the low concentration of magnetite in situ—a few parts per billion (*22*).

We determined the presence and nature of the magnetite in honeybee trophocytes by examining the fine structure of the iron granules in the trophocytes with high-resolution transmission electron microscopy (HRTEM). Adult worker bees, 25 to 35 days after eclosion, were dissected, fixed, and embedded according to the conventional procedure (*21*). Thin sections were cut with a diamond knife and stained with uranyl acetate and lead citrate (*21*). Forty iron granules (Fig. 1A) (from five bees) with an average diameter of 0.6 μm were analyzed by a JEOL 4000EX HRTEM operating at 400 kV. Crystals were found in the central portion of four of the examined iron granules. The crystallized central portion occupied 30% of the granule volume. The largest crystal was approximately 10 nm in diameter. The direction of lattice structure in nearby crystals was random, and the lattice fringes often appeared to extend across the region of 7.5-nm electron-dense particles (Fig. 1B). A diffraction pattern (Fig. 1D) was obtained from a lattice image (Fig. 1C) by Fourier transformation. The *d*-spacings calculated from the diffraction pattern were consistent with the [1 $\bar{2}$ 1] zone axis pattern of magnetite (*23*). All of the magnetite crystals showed well-ordered lattice planes, and none of the crystals had any other crystalline phases, such as those typical of γ-FeOOH. Previous investigators may not have obtained diffraction patterns from these crystals because of the crystals' small size.

If the observed superparamagnetic granules are indeed the honeybees' magnetoreceptors, then nervous system innervation of the trophocytes would be expected. The abdominal areas of adult worker bees, 25 to

C.-Y. Hsu, Institute of Life Science, National Tsing Hua University, Hsinchu, Taiwan, Republic of China.
C.-W. Li, Institute of Life Science, National Tsing Hua University, Hsinchu, and National Museum of Natural Science, Taichung, Taiwan, Republic of China.

*To whom correspondence should be addressed at National Tsing Hua University.

35 days after eclosion, were carefully dissected so as to minimize disruption of the abdomen. The abdomens were then fixed with glutaraldehyde and osmium tetroxide, dehydrated through an ethanol series, and dried on a Hitachi HCP-2 critical point dryer. Their structure was then examined by scanning electron microscopy. The ventral nerve cord that runs along the longitudinal axis of the honeybee consists of a segmented chain of stereotypical ganglia. A bundle of axons extended laterally from each ganglion to innervate a cluster of trophocytes (Fig. 2A). Neuron processes were embedded in the trophocytes (Fig. 2B). A synaptic terminal with synaptic vesicles of various electron densities was found in close proximity to the membrane of a trophocyte (Fig. 2C). The cytoskeleton associated with the membrane of iron granule vesicles contained filaments 8 to 10 nm in diameter, which suggests the presence of microfilaments or intermediate filaments (Fig. 2D).

The estimated number of superparamagnetic particles can be calculated on the basis of iron granule size. The volume of the average iron granule with a diameter of 0.6 μm is 1.13×10^{-13} ml. The superparamagnetic particles occupy approximately 13% of the crystallized central portion, which constitutes 30% of the granule volume. The estimated volume of the superparamagnetic particles is 4.4×10^{-15} ml per iron granule. The volume of superparamagnetic particles that are 10 nm in diameter is 5.2×10^{-19} ml. Thus, the estimated number of superparamagnetic particles is approximately 8.5×10^{3} per iron granule.

A working hypothesis for magnetoperception in honeybees can be formulated on the basis of our findings. External magnetic fields may cause expansion or contraction of the superparamagnetic particles, depending on their orientation. In one orientation, the particles would be in a side-by-side position, creating repulsion and the subsequent expansion of the iron granule. In the other orientation, particles would be positioned end to end, creating attraction and the subsequent contraction of the iron granule (*24, 25*). The associated cytoskeleton might relay the signal in a mechanism similar to that which transduces the signal of statoliths in the root apical cells of plants (*26*). The signal, magnified by gap junctions (*27*), may trigger the release of synaptic terminal vesicles, initiating a neural response.

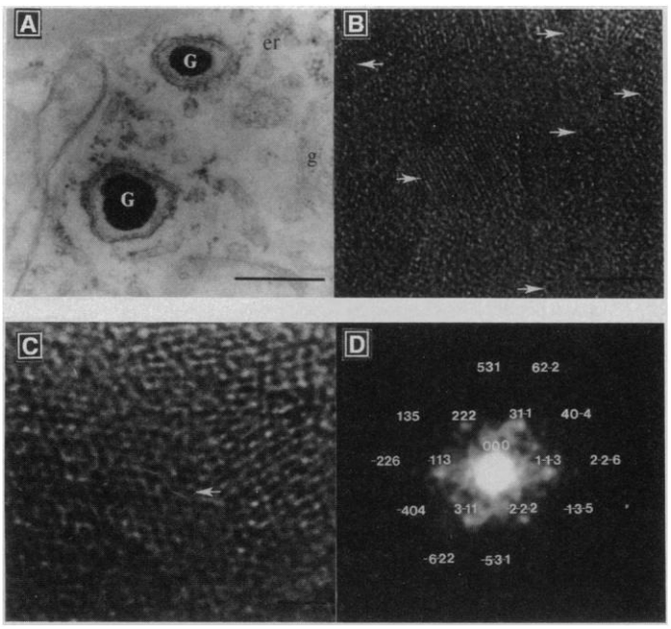

Fig. 1. (**A**) Aggregation of the 7.5-nm dense particles forms a core granule (G) in an iron deposition vesicle. Abbreviations: er, endoplasmic reticulum; g, Golgi apparatus. Scale bar, 0.4 μm. (**B**) HRTEM micrograph of the central portion of an iron granule, showing the coexistence of crystalline (arrows) and noncrystalline regions. Scale bar, 3.5 nm. (**C**) HRTEM micrograph of an individual crystal, showing well-ordered fringes. The arrow denotes the selected area of the electron diffraction pattern shown in (D). Scale bar, 1 nm. (**D**) Electron diffraction pattern from the lattice image, obtained by Fourier transformation. The pattern corresponds to the [1 $\bar{2}$ 1] zone of magnetite.

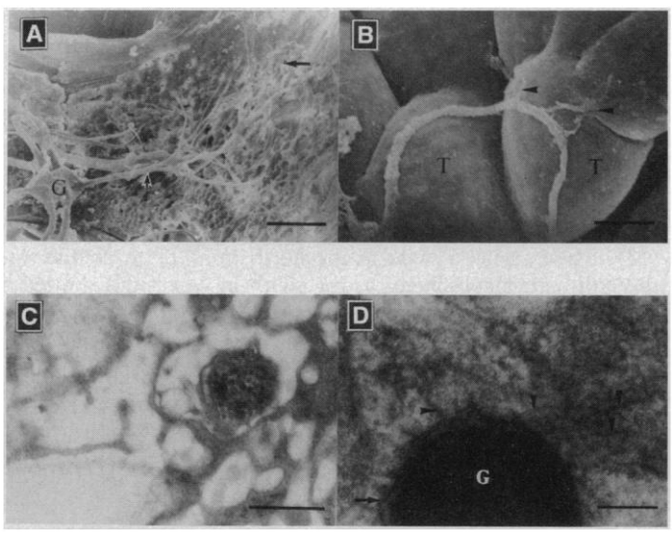

Fig. 2. (**A**) Scanning electron micrograph of a bundle of axons (arrowhead) laterally branching from a ganglion (G) to innervate a cluster of trophocytes (arrow). Scale bar, 0.3 mm. (**B**) Scanning electron micrograph of nerve processes, showing nerve endings (arrowheads) innervating trophocytes (T). Scale bar, 20 μm. (**C**) Transmission electron micrograph of a synaptic terminal associated with a trophocyte. Scale bar, 0.5 μm. (**D**) Transmission electron micrograph showing cytoskeletal filaments (arrowheads) attached to the membrane (arrow) of an iron deposition vesicle. G, iron granule. Scale bar, 90 nm.

REFERENCES AND NOTES

1. R. Blakemore, *Science* **190**, 377 (1975).
2. F. F. Torres De Araujo, M. A. Pires, R. B. Frankel, C. E. M. Bicudo, *Biophys. J.* **50**, 375 (1985).
3. K. J. Lohmann and A. O. D. Willows, *Science* **235**, 331 (1987).
4. H. Martin and M. Lindauer, *J. Comp. Physiol. A* **122**, 145 (1977).
5. M. Kisliuk and J. Ishay, *Experientia* **33**, 885 (1977).
6. T. P. Quinn and E. L. Brannon, *J. Comp. Physiol. A* **147**, 547 (1982).
7. M. M. Walker, *ibid.* **155**, 673 (1984).
8. A. Perry, G. B. Bauer, A. E. Dizon, in *Magnetite Biomineralization and Magnetoreception in Organisms: A New Biomagnetism*, J. L. Kirschvink, D. S. Jones, B. J. MacFadden, Eds. (Plenum, New York, 1985), pp. 439–453.
9. J. B. Phillips, *J. Comp. Physiol. A* **121**, 273 (1977).
10. C. Walcott and R. P. Green, *Science* **184**, 180 (1974).
11. J. L. Kirschvink, A. E. Dizon, J. A. Westphal, *J. Exp. Biol.* **120**, 1 (1986).
12. R. R. Baker, *Science* **210**, 555 (1980).
13. K. H. Towe and T. T. Moench, *Earth Planet. Sci. Lett.* **52**, 213 (1981).
14. R. P. Blakemore and R. B. Frankel, *Sci. Am.* **245**, 58 (December 1981).
15. M. M. Walker, J. L. Kirschvink, S.-B. R. Chang, A. E. Dizon, *Science* **224**, 751 (1984).
16. J. L. Kirschvink, M. M. Walker, S.-B. R. Chang, A. E. Dizon, K. A. Peterson, *J. Comp. Physiol. A* **157**, 375 (1985).
17. S. Mann, N. H. C. Sparks, M. M. Walker, J. L. Kirschvink, *J. Exp. Biol.* **140**, 35 (1988).
18. J. L. Kirschvink, A. Kobayashi-Kirschvink, B. J. Woodford, *Proc. Natl. Acad. Sci. U.S.A.* **89**, 7683 (1992).
19. J. L. Gould, J. L. Kirschvink, K. S. Deffeyes, *Science* **201**, 1026 (1978).
20. D. A. Kuterbach, B. Walcott, R. J. Reeder, R. B. Frankel, *ibid.* **218**, 695 (1982).
21. C.-Y. Hsu and C.-W. Li, *J. Exp. Biol.* **180**, 1 (1993).
22. J. L. Kirschvink, *Bioelectromagnetics* **10**, 239 (1989).
23. [1 $\bar{2}$ 1] is the direction of the electron beam and is obtained by the cross product of [3 1 $\bar{1}$] and [1 $\bar{1}$ $\bar{3}$] [see P. Hirsch, A. Howie, R. B. Nicholson, D. W. Pashley, M. J. Whelan, *Electron Microscopy of Thin Crystals* (Krieger, New York, 1977)].
24. W. F. Towne and J. L. Gould, in *Magnetite Biomineralization and Magnetoreception in Organisms: A New Biomagnetism*, J. L. Kirschvink, D.

S. Jones, B. J. MacFadden, Eds. (Plenum, New York, 1985), pp. 385–406.
25. J. L. Kirschvink and J. L. Gould, *Biosystems* **13**, 181 (1981).
26. A. Sievers, S. Kruse, L.-L. Kuo-Huang, M. Wendt, *Planta* **172**, 321 (1989).
27. D. A. Kuterbach and B. Walcott, *J. Exp. Biol.* **126**, 375 (1986).
28. We thank F. R. Chen for technical help and discussions and P. C. Huang for discussions and critical reading of the manuscript. Supported by the National Science Council, Republic of China.

11 January 1994; accepted 5 May 1994

Ecosystem Response to Solar Ultraviolet-B Radiation: Influence of Trophic-Level Interactions

Max L. Bothwell,* Darren M. J. Sherbot, Colleen M. Pollock

Solar ultraviolet radiation (UVR) can reduce the photosynthesis and growth of benthic diatom communities in shallow freshwater. Nevertheless, greater amounts of algae accumulate in UVR-exposed habitats than in UVR-protected environments. Near-ultraviolet (UVA wavelengths of 320 to 400 nanometers) and mid-ultraviolet (UVB, wavelengths of 280 to 320 nanometers) radiation also inhibit algal consumers (Diptera: Chironomidae). Larval chironomids are more sensitive to UVB than sympatric algae. Differential sensitivity to UVB between algae and herbivores contributes to counterintuitive increases in algae in habitats exposed to UVB. These mesocosm experiments illustrate that predictions of the response of entire ecosystems to elevated UVB cannot be made on single trophic-level assessments.

Solar ultraviolet radiation (UVR: 280 to 400 nm) at mid-latitudes during the summer can inhibit algal photosynthesis in oceans and lakes (*1–5*). Middle ultraviolet radiation (UVB: 280 to 320 nm) disrupts many photosynthetic processes including the electron transport system (*6*), photosystem II reaction centers (*7*), and pigment stability (*8*). It also damages algal DNA (*9, 10*), and both UVB and near-ultraviolet radiation (UVA: 320 to 400 nm) reduce algal growth rates (*11, 12*). Short-term UVR-screening experiments confirm the UVR inhibition of attached diatom growth rates during the summer at mid-northern latitudes (*13*). Paradoxically, extended exposure to UVR substantially increased the diatom biomass (*13*). Furthermore, lower intensities of UVR, non-inhibiting to the algal accrual rate, also augmented autotrophic biomass accumulation when compared to habitats completely shielded from UVR (*13*).

Algae can increase their tolerance of UVR by synthesizing protective UVR-absorbing compounds (*14*) and by repairing damaged DNA (*9, 10*). A wide range in sensitivity to UVR exists among algal taxa (*9, 11*). Succession to algal species presumed to be more UVR-tolerant has been documented in longer experiments (*13, 15*). However, succession, physiological adaptation, or both could not explain the more than doubling of algal biomass in response to UVR exposure observed in our earlier experiments (*13*). Discrepancies between short- and long-term effects of UVR on algae have been observed and reported (*16, 17*). Severe photosynthetic inhibition and DNA damage documented in short-term exposures of Antarctic phytoplankton to near-surface levels of UVB did not lower algal growth rates or reduce algal accumulation over extended periods of time (*16, 17*). Mesocosms with freshwater plankton communities in Lake Negra (Chile) exposed to near-surface, full-spectrum sunlight for 20 days supported greater algal biomass than communities protected from UVR (*18*). Similar observations of elevated phytoplankton in mesocosms exposed to UVR have recently been made in North America (*19*).

Middle ultraviolet radiation can affect organisms at all trophic levels, both directly and indirectly (*1, 20*). Thus, compounding

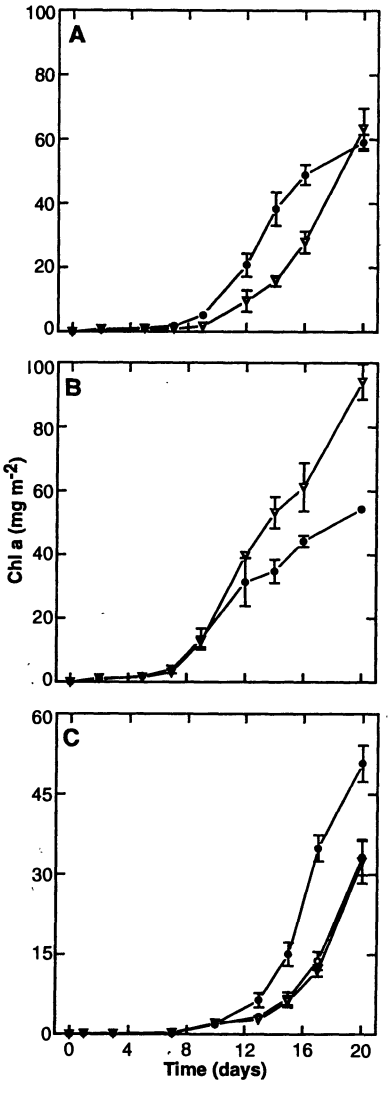

Fig. 1. (**A**) UVR inhibition of algal (Chl a) community growth and accrual by 90% PAR+UVA+UVB (PVI, inverted triangles) compared to growth under 90% PAR (UF-1, closed circles). During the initial 1 to 2 weeks, specific growth rates were lowered by UVR (*13*) (ANCOVA, $P < 0.01$). Reduced growth rates resulted in lower accrued Chl a and algal biomass (cell volumes) during this initial phase (*13*) (ANOVA, $P < 0.05$). After 3 weeks, algal biomass (Chl *a* and cell volume) in PAR+UVA+UVB exceeded that under PAR two- to fourfold (*13*). Initial UVR growth inhibition was eliminated by either (**B**) a reduction in ambient sunlight by 50% with neutral density screens [under 10 days, 50% (UF-1) PAR = 50% PAR+UVA+UVB (PVI) (ANCOVA, $P > 0.05$) or (**C**) the selective screening out of UVA [90% PAR (UF-4, closed circles) 90% PAR+UVA (Mylar, open circles) (ANCOVA, $P < 0.05$) (PAR+UVA+UVB: OP-4, inverted triangles)]. Removal of UVB had no effect on algal accrual rate [90% PAR+UVA+UVB = 90% PAR+UVA (ANCOVA, $P >> 0.05$)]. The 50% reduction in ambient sunlight intensity (B) also eventually resulted in higher algal biomass under PAR+UVA+UVB than under PAR. Mean incident UVB levels were 48.8 kJ m^{-2} d^{-1} (A and B) and 53 kJ m^{-2} d^{-1} (C). Mean incident UVA was 888 kJ m^{-2} d^{-1} during the 1992 trial. Mean daily PAR levels during the trials were 39.8 E m^{-2} d^{-1} and 36.3 E m^{-2} d^{-1} for 1991 and 1992, respectively. Error bars are ±SEM.

M. L. Bothwell, National Water Research Institute, Burlington, ON L7R 4A6, and National Hydrology Research Institute, Saskatoon, SK S7N 3H5, Canada. D. M. J. Sherbot and C. M. Pollock, National Hydrology Research Institute, Saskatoon, SK S7N 3H5, Canada.

*To whom correspondence should be addressed at the National Hydrology Research Institute, Saskatoon, SK S7N 3H5, Canada.